PERGAMON

International Journal of Multiphase Flow 25 (1999) 841–855

International Journal of Multiphase Flow

www.elsevier.com/locate/ijmulflow

A model for calculation of steam injector performance

N. Deberne[a,*], J.F. Leone[a], A. Duque[b], A. Lallemand[a]

[a]CETHIL, UPRESA CNRS 5008, INSA Lyon, 20 avenue Albert Einstein, 69621 Villeurbanne cedex, France
[b]EDF/SEPTEN, 12–14 Avenue Dutrievoz, 69628 Villeurbanne Cedex, France

Received 4 August 1997; received in revised form 20 October 1998

Abstract

Steam injectors can be used in many applications, but especially for security water injection in steam generators of nuclear reactors. Using a one-dimensional model, a steam injector with a centered liquid supply has been simulated. General relationships are presented from the nozzle exit to the steam injector outlet. It is shown that the flow contains a condensation shock. To achieve modelling of the mixing zone, and empirical correlation giving an equivalent pressure with value of condensation rate is found using experimental results obtained at the CETHIL. A parametric study is then made to determine the influence of significant parameters and the functioning range of the steam injector. Calculated values are compared with experimental results and are found to be in good agreement.

Keywords: Steam injector; Jet pump; Condensing injector; Ejector condenser

1. Introduction

A steam injector is a device whereby steam is used to pump cold water at low pressure and to produce an outlet water pressure which is higher than the steam inlet pressure. Its main characteristic is that no moving parts are needed for its functioning, thermodynamic processes relying on direct transfers of mass, momentum and heat between the two phases.

The steam injector can be used as a safety pump in a light water reactor, as a steam supply is generally available in power plants and a high pressure water supply can be useful for heat removal in case of incident. Moreover, it is a passive system without rotating machinery and its functioning requires no external energy supply.

* Corresponding author.

0301-9322/99/$ - see front matter
PII: S0301-9322(98)00071-8

A simplified steam injector schematic, divided into five regions, is shown in Fig. 1. In the first part, called the steam nozzle (a), having a converging-diverging shape, the steam is accelerated to supersonic velocity through a nearly isentropic expansion. Water is distributed by the water nozzle or the liquid injector (b). Here, the chosen arrangement is a central water nozzle and an annular outer steam nozzle. In our study, it will be seen that the geometrical arrangement has an effect on the results, but it can be inverted with a small modification to the model. In the mixing section (c), steam and water exchange heat, momentum (due to temperature and velocity differences) and mass (due to condensation of steam on the water droplets extracted from the water cone at the exit of the water nozzle). Condensation is achieved in the shock wave (d) occurring at the exit of the mixing section. The major pressure rise is realized in this shock wave. Then, the water is decelerated in the diffuser (e) and kinetic energy is converted into a further pressure increase.

Although the technology of the steam injector has been known for about a century, its modelling still represents an incompletely solved problem. Experiments have been previously carried out by Rose (1960), Grolmes (1968) and Alad'yev et al. (1981a, b). More recently, its possible use for nuclear power plants has involved new studies by Manno and Dehbi (1990), Narabayashi et al. (1991), Leone et al. (1994, 1995) and Cattadori et al. (1991).

Two kinds of model can be used for the calculation of steam injector performances. The first approach (called the local model) consists of modelling the flow in the injector at each point, taking into account major phenomena (such as, for example, condensation of droplets, heat and momentum transfers, viscous dissipation on the wall non-adiabatic and non-equilibrium flow). Such a model is more realistic, but needs a perfect knowledge of the previously mentioned phenomena as well as their mutual interactions. Unfortunately, these models are not yet predictive due to the complexity of the flow in the mixing chamber.

The second approach (called the global model) consists of considering a large control volume in which one-dimensional conservation equations are applied. This kind of model is simpler than the previous one but is less realistic. Irreversibilities are often taken into account using empirical factors (in order to obtain calculated data fitting experimental values), which cannot really be justified. Moreover, these factors are only known for one experimental condition and cannot be generalized.

In this paper, a global model is employed but, instead of using correcting empirical factors, irreversibilities are taken into account through the pressure variation along the mixing section. It appears that, for the central water nozzle arrangement, pressure variations can be easily modelled depending on the condensation rate in the mixing section. Moreover, the two phases

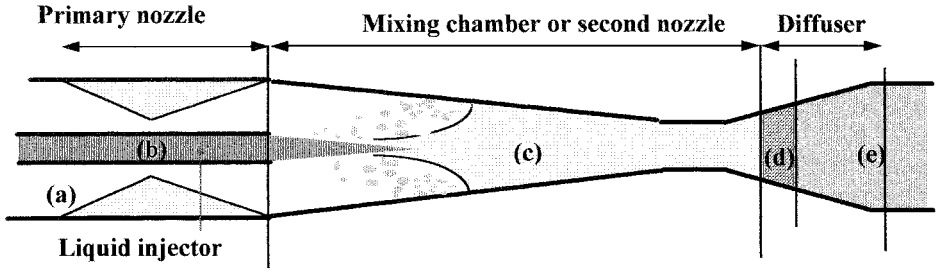

Fig. 1. Schematic sketch of steam injector.

are considered separately and the shock wave and the mixing section are modelled apart. Closure of the equation set is ensured by equilibrium assumptions at the exit of the mixing section and by a condition of complete condensation downstream of the shock. Properties of water are calculated with software created at the CETHIL based on the Schmidt (1969) formulation. This approach is entirely original and can be used without acquiring any previous experimental data.

A parametric study is then used to determine the influence of significant parameters and the functioning range of the steam injector. Calculated values are compared with experiments performed at the CETHIL and are found to be in good agreement.

2. Steam injector modelling

Modelling of the steam nozzle (a) and water nozzle (b) is not presented in this paper, as the fluids states depend on the arrangement of pipes in the rig. In the converging–diverging steam nozzle, a supersonic flow is obtained and steam state is supposed to be known at the mixing section inlet. The subscript referring to this plane will be noted 1s. In the same way, subscripts 1l, 2, 3 and 4 will respectively define the water mixing section inlet (water nozzle outlet), the mixing section outlet, the shock wave outlet and the diffuser outlet planes. It should be pointed out that in plane (2), both steam and water are present so subscripts 2s and 2l will be used, but will not correspond to separate phases as in (1s) and (1l). The flow is assumed to be steady and one-dimensional.

2.1. Modelling of the mixing section

The mixing section is the most important part of the steam injector, where momentum, mass and heat transfers between phases take place. Two kinds of flows can be observed in the mixing section: a stratified flow in the upstream region, consisting of a liquid jet surrounded by wet steam and a downstream homogeneous two-phase flow. The liquid jet is gradually disintegrated into small droplets by the supersonic flow of steam until it completely vanishes. In this first region, momentum transfer is very important. When the flow is a homogeneous mixture of liquid and steam, the exchange surface is greater and the mass and heat transfers are thus increased.

In our system, pressure is assumed to be equal to the steam pressure, which is a well-known assumption in most two-phase flow configurations. Consequently, it is assumed $P_S = P_L$ in the mixing chamber.

At the end of the mixing section, spray flow was confirmed by visualization experiments and, a posteriori, with analysis of the void fraction. Numerical calculations give a range of vapour quality from 0.05 to 0.4. Consequently, the assumption of equal velocities of steam and water $u_{2\,s} = u_{2\,l} = u_2$ at the end of the mixing section is realistic.

It will also be assumed that thermal equilibrium is reached at the end of the mixing section, so that $T_{2\,s} = T_{2\,l} = T_2$. This assumption made by Rose (1960), Grolmes (1968) and Alad'yev et al. (1981a, b) is realistic if the mixing section is more than about seven times the exit diameter of the liquid injector.

The heat and momentum transfers are very fast with a time scale shorter than the transit time of the flow. This assumption was experimentally verified by Myazaki et al. (1973) who measured the static temperature and pressure along the mixing chamber. Their results show that the flow is near to the saturation everywhere (except in the condensation shock) with heat transfer coefficients of about 10^6 W/m^2 K.

The external losses due to viscous forces on the section wall and thermal losses (non-adiabatic wall) will be neglected (Rose, 1960; Grolmes, 1968). By calculating the global entropy production due to internal and external heat and momentum transfers, we show that the main irreversibilities are created by the non-equilibrium flow which generates more dissipation than the external losses. These assumptions were easily verified by introducing viscous and wall thermal loss terms into the momentum and the energy equations.

Conservation equations applied to the global volume (V) (Fig. 2) lead to:

Mass

$$\rho_2 u_2 = (1+U)\frac{1}{\Omega}\epsilon_1 \rho_{1s} u_{1s} \tag{1}$$

with

$$\epsilon_1 = \frac{1}{\left(U\frac{\rho_{1s}u_{1s}}{\rho_{1l}u_{1l}}+1\right)} \quad \text{inlet void fraction}$$

$$\Omega = \frac{S_2}{(S_{1s}+S_{1l})} \quad \text{area contraction ratio}$$

ρ = density, S = area, $U = M_l/M_S$ mass flow rate ratio, deduced from the inlet conditions at the mixing chamber.

Momentum

$$(1+U)u_2 + \frac{\Omega}{\epsilon_{1s}\rho_{1s}u_{1s}}\left(P_2 + \left(1-\frac{1}{\Omega}\right)P*\right) = (u_{1s}+Uu_{1s}) + \frac{P_{1s}}{\epsilon_1\rho_{1s}u_{1s}} \tag{2}$$

where

$$P* = \frac{\int_1^2 P(\mathbf{n}\cdot\mathbf{z})\,\mathrm{d}A}{\int_1^2(\mathbf{n}\cdot\mathbf{z})\,\mathrm{d}A} = \frac{1}{(S_2-S_1)}\int_1^2 P(\mathbf{n}\cdot\mathbf{z})\,\mathrm{d}A \tag{3}$$

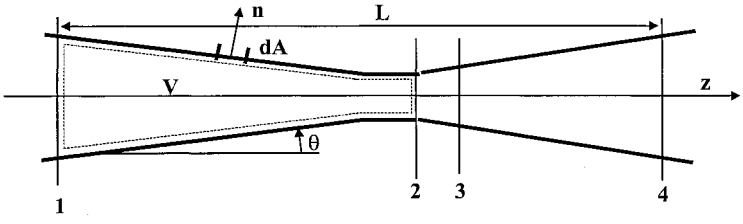

Fig. 2. Control volume for the modelling of the mixing chamber.

$$dA = -\frac{2\pi r(z)}{\cos\theta(z)}\,dz$$

$r(z)$ being the mixing section radius at location z, **n** being the normal unitary vector. P^*, called the equivalent pressure, is the average static pressure along the mixing chamber and reflects the main internal irreversibilities of the flow.

Energy

$$(1+U)\left[h_2+\frac{u_2^2}{2}\right] = U\left[h_{1l}+\frac{u_{1l}^2}{2}\right]+\left[h_{1s}+\frac{u_{1s}^2}{2}\right] \tag{4}$$

h is the specific enthalpy.

State equation

$$h_2 = h(P_2, \rho_2). \tag{5}$$

The unknown quantities are ρ_2, u_2, P_2, h_2 and the system of Eqs. (1) + (2) + (4) + (5) is closed only if the term P^* is known.

2.2. Determination of the equivalent pressure P^*

The equivalent pressure depends on the pressure profile along the wall of the mixing section and must be determined for complete modelling of the mixing section. It seems that, for an arrangement with a central liquid nozzle and an annular steam nozzle, similar pressure profiles can be found with experimental results (Grolmes, 1968; Alad'yev et al., 1981a,b). At the beginning of the mixing section, the pressure decreases due to fluid acceleration. Downstream of this region, the pressure increases reaching a maximal value P_{max} at distance z_{bu}. Grolmes (1968) found that this distance is related to the break-up of the liquid jet, when its disintegration is achieved. While the flow is stratified, condensation is not very important, the interphase surface being small. The pressure is altered both by the decrease of cross sectional area and the deceleration of fluid and thus increases. When the flow is homogeneous (downstream of z_{bu}), the pressure is altered by the high condensation rate which involves a drop in specific volume and a pressure decrease which is more important than the increase due to the mixing section convergence. Grolmes (1968) defined a condensation rate:

$$R = \left(\frac{x_1 L_v}{c_{pl}\Delta T U}\right)_{P_1} \tag{6}$$

where $\Delta T = T_{sat} - T_{1\,1}$ (T_{sat} saturation temperature at pressure P) is the inlet liquid subcooling, L_v is the latent heat of water, c_{pl} is the heat capacity of liquid and x_1 is the vapour quality at the mixing inlet section. It has been shown by Grolmes (1968) that the experimental pressure profile depends on this condensation rate. Figs. 3 and 4 show pressure profiles measured on our experimental loop (see Section 3) inside the mixing section as a function of distance from inlet, respectively for several values of R and for several values of back-pressure. It can be seen that:

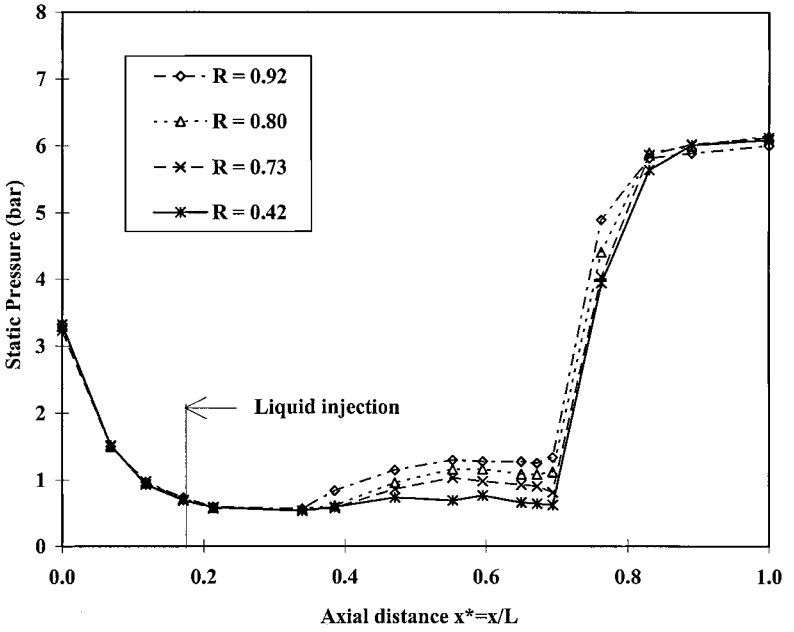

Fig. 3. Pressure profiles for several condensation rates and for fixed back-pressure.

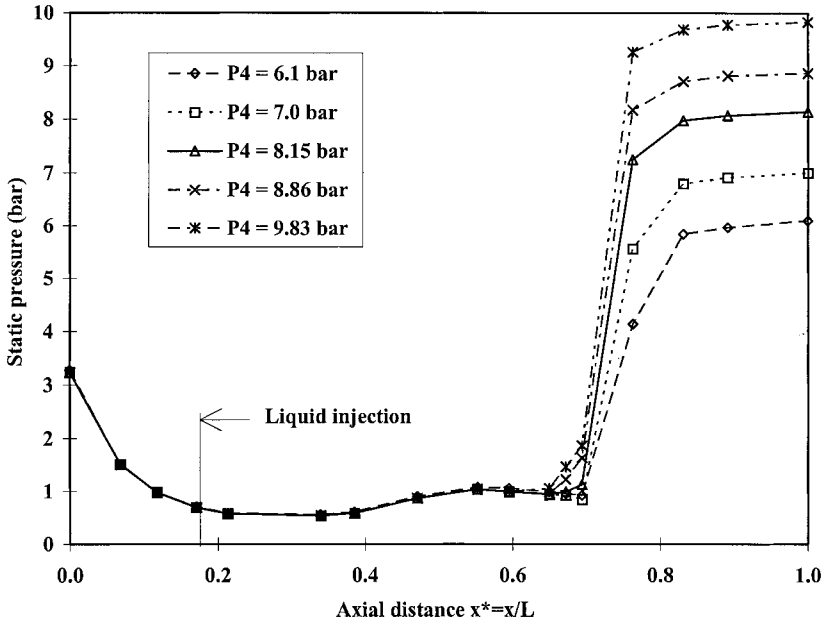

Fig. 4. Pressure profiles for several back-pressure and for fixed inlet parameters ($P_{0\,1} = P_{0\,s} = 6$ bar; $T_{0\,1} = 23°C$).

- the maximal pressure P_{max} decreases with the condensation rate. Grolmes (1968) showed that for $R < 0.69$, the pressure is nearly constant along the wall;
- the back-pressure has no influence on the flow before the condensation shock which confirms that the behaviour of the flow in the mixing chamber is supersonic.

In order to correlate the equivalent pressure with the condensation rate ($R > 0.69$), we define the pressure ratio:

$$\tau* = \frac{P*}{P_{1s}} \tag{7}$$

Equivalent pressures $P*$ are obtained by numerically integrating the experimental measurements of static pressure along the mixing chamber obtained at the CETHIL. By correlating these results with the condensation rate, we find an empirical expression for $\tau*$ (Fig. 5):

$$\tau* = 1.01R^{2.572} \tag{8}$$

Taking into account the dependence of the pressure profiles as a function of the condensation rate, we also use two methods for calculating the equivalent pressure and closing the model:

- *Method 1*: for $R > 0.69$, $P*$ is deduced from the empirical correlation (8);
- *Method 2*: for $R < 0.69$, Grolmes (1968) found that pressure is constant along the wall of the mixing section. Instead of considering a constant pressure, we will only assume that the profile is linear between planes 1 and 2. The equivalent pressure is obtained by integrating the expression (9):

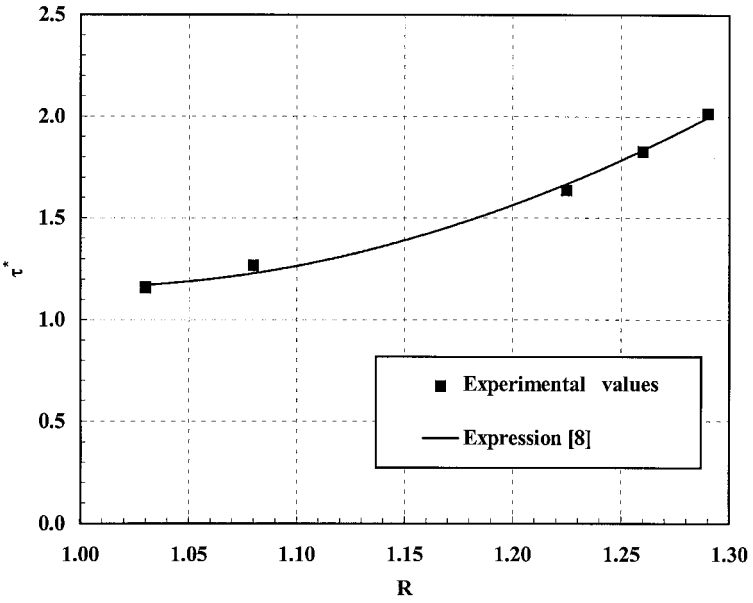

Fig. 5. Correlation for equivalent pressure rate as a function of the condensation rate.

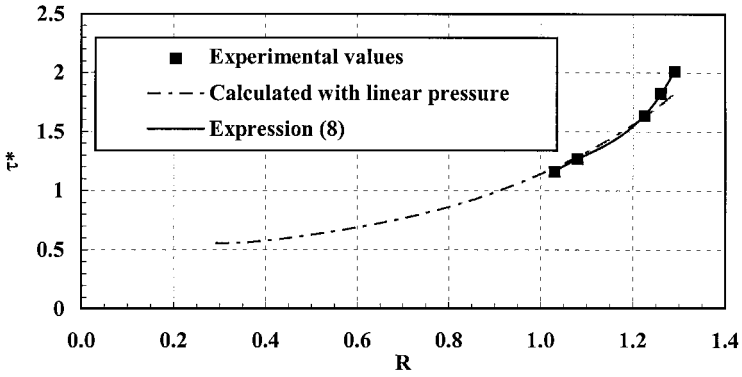

Fig. 6. Comparison between two methods for calculation of τ^*.

$$P(z) = \frac{(P_2 - P_{1s})}{(z_2 - z_1)}(z - z_1) + P_{1s} \tag{9}$$

Calculations of P^* seem to be correct for values of R extrapolated up to 1.1, although the hypothesis itself is no longer valid (Fig. 6). It shows that the transition between the two methods is sufficiently smooth.

This method is only valid for the central water nozzle–annular outer steam nozzle arrangement. In the case where the two nozzles are inverted, a new method for calculating P^* has to be found, but formulation of the model is the same.

2.3. Modelling of the shock wave

The shock wave obtained in a steam injector occurs in a two-phase fluid and involves a complete condensation. Consequently, the fluid which is downstream of the wave is assumed to be only liquid. Studies about this kind of flow are nearly non-existent. More references exist on vapour-droplet flows, when the void fraction is more important.

The functioning of the steam injector, depending on the void fraction, will be bounded by two limiting cases. If the void fraction is too high, the fluid will not be condensed enough to reach a complete condensation across the shock wave. In the opposite case if the void fraction is too low, the fluid velocity will be too low (lower than the sound speed) and no shock wave can occur. Saltanov et al. (1970) found the following expression for the minimal void fraction:

$$\epsilon_{\min} = \frac{1 - \frac{\rho_3}{\rho_{2l}}}{1 - \frac{\rho_{2s}}{\rho_{2l}}} \tag{10}$$

In a two-phase flow, Young and Guha (1991) define two asymptotic sound speeds. Depending on the steam velocity, compared with these sound speeds, the normal shock wave structure occurring in an injector can be divided into two main categories.

The first sound speed, called the frozen sound speed because it corresponds to the case where response of droplets is negligible (droplets are frozen with no mass and momentum transfers), is similar to the sound speed in pure gases:

$$a_f = \sqrt{\gamma R_g T_s} \tag{11}$$

where γ is the ratio of the specific heat capacities and R_g is the specific gas constant, for the vapour phase.

The other sound speed, presented in Young and Guha (1991), is called the full equilibrium sound speed, where all processes are in equilibrium during shock wave:

$$a_e = \sqrt{\frac{x\gamma R_g T_s}{\gamma\left[1 - \frac{R_g T_s}{L_v}\left(2 - \frac{cT_s}{L_v}\right)\right]}} \tag{12}$$

with $c = c_{ps} + ((1-\epsilon)/(\epsilon))c_{pl}$. It can be seen that the condition $\epsilon > \epsilon_{min}$ prevents expression of c from divergence.

It appears that, in order to obtain a normal shock wave, the upstream steam velocity must be higher than the full equilibrium sound speed, so that in the present case: $u_2 > a_e$. If u_2 is between a_e and a_f, the shock wave is fully dispersed and presents no discontinuity in flow properties. If the upstream steam velocity is higher than the frozen sound speed ($u_2 > a_f$), the shock wave is partly dispersed.

A discontinuity appears, followed by a continuous relaxation zone. Fig. 4 shows experimental pressure profiles across the shock wave and for different back-pressures. The number and locations of the pressure tappings do not ensure a perfect knowledge of the pressure profile. However, if a fully dispersed typical profile seems to fit adequately experimental data, a partly dispersed profile seems to be less natural. Experimental pressure profiles across the normal shock wave obtained by Grolmes (1968) with more pressure taps give similar results. For this reason, our modelling of the shock wave supposes that equilibrium of flow properties is reached at the end of the shock wave, permitting use of the equation of state at this point. The position of the shock wave has been fixed at the throat of the nozzle, because it is the case where maximum outlet pressure P_4 is obtained and therefore the optimal performance of the steam injector for given inlet conditions.

Flow is assumed to be two-phase upstream of the shock and liquid downstream. The angle of divergence of the diffuser and the shock thickness are sufficiently small to neglect the effect of the wall on the wave and surface areas of Sections 2 and 3 are taken to be equal ($S_2 = S_3$). This assumption was numerically verified.

Mass

$$\rho_3 u_3 = \rho_2 u_2 \quad \text{with} \quad \rho_2 = \epsilon\rho_{2s} + (1-\epsilon)\rho_{2l} \quad \text{average density} \tag{13}$$

Momentum

$$\rho_3 u_3^2 + P_3 = \rho_2 u_2^2 + P_2 \tag{14}$$

Energy

$$\rho_3 u_3\left(h_3 + \frac{1}{2}u_3^2\right) = \rho_2\frac{u_2^3}{2} + u_2[\epsilon_2\rho_{2s}h_{2s} + (1-\epsilon_2)\rho_{2l}h_{2l}] \tag{15}$$

State equation

$$h_3 = h(P_3, \rho_3) \tag{16}$$

2.4. Modelling of the diffuser

The flow inside the diffuser is incompressible ($\rho_3 = \rho_4$) because of the liquid phase. The diffuser simply changes kinetic energy into pressure. Because of the high liquid velocities at the exit of the throat, we introduce a pressure loss term in the Bernoulli equation:

Mass

$$S_4 u_4 = S_3 u_3 \tag{17}$$

Bernoulli equation

$$P_4 + \frac{1}{2}\rho_3 u_4^2 = P_3 + \frac{1}{2}\rho_3 u_3^2 - C_D \rho_3 u_3^2 \tag{18}$$

where C_D is the loss coefficient for the conical diffuser, calculated from Idel'cik (1986).

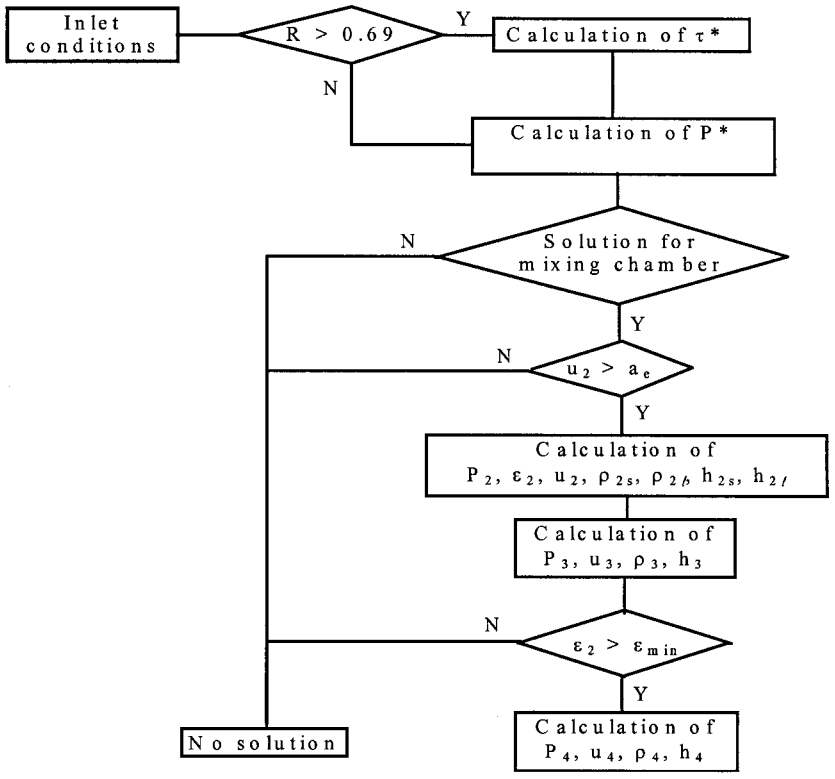

Fig. 7. Schematic of the model.

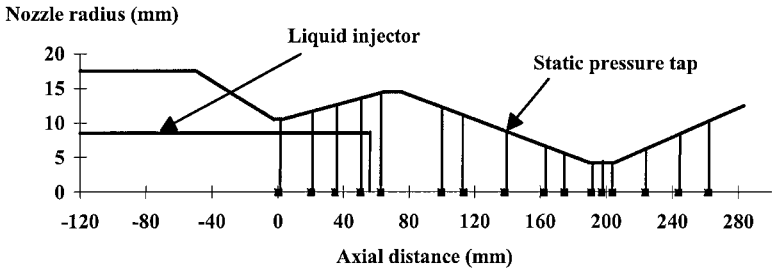

Fig. 8. Steam injector used for experiments.

2.5. Outline of the calculation scheme

A flow chart for the calculation scheme is presented on Fig. 7. Once the inlet conditions are known, as well as the steam injector geometry (Fig. 8), the condensation rate R is calculated. The term P^* is calculated with the equivalent pressure ratio τ^* and then all the other constants. If a solution for the system of Eqs. (1) + (2) + (4) + (5) cannot be found, the calculation aborts if the flow velocity u_2 is lower than sound speed upstream of the shock wave. This restriction does not mean that no flow can occur, but that the assumptions (two-phase supersonic upstream flow, shock wave and liquid downstream flow) cannot be ensured. Physical quantities of the flow are then calculated upstream and downstream of the shock wave and the minimum void fraction condition (10) is a posteriori verified (to be sure that a normal shock wave exists). The outlet quantities are, in this case, calculated.

3. Description of experimental apparatus

The area contraction ratio Ω of the tested injector is equal to 1/12. The influence of the inlet parameters has been studied separately. The test equipment operates in a closed loop (Fig. 9), where it is possible to independently vary the steam pressure, liquid temperature, liquid flow rate and back-pressure. The parameter ranges are given in Table 1.

The steam and water flow rates were measured by means of calibrated orifice plate and multiple Pitot tube (Annubar), respectively. Temperatures and pressures were measured by K-type thermocouples and by resistive pressure transducers, respectively. The axial pressure profiles in the steam nozzle, mixing chamber and diffuser were measured by thin film-type pressure transducers. The steam inlet pressure was varied by means of a control valve.

The start-up procedure includes three stages:

1. The steam valve is closed and the liquid valve and drain are open; the drain is a discharge port connected to the atmosphere or to a condenser.
2. The steam valve is progressively opened.
3. When the primary nozzle is started, the drain valve is closed.

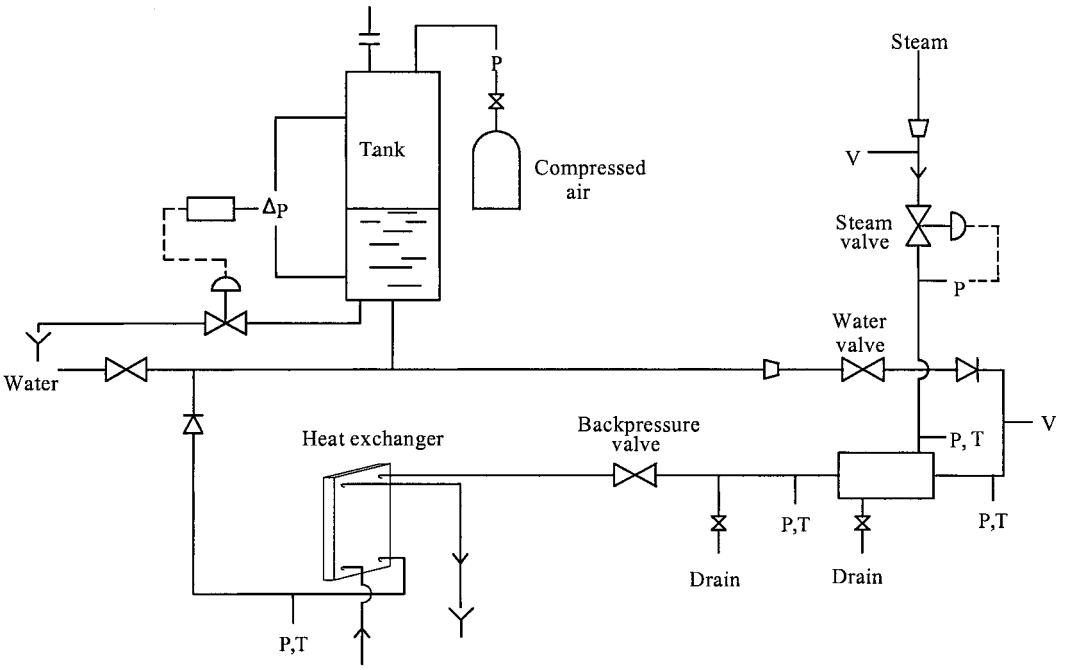

Fig. 9. Schematic of the test facility.

It is not possible to start the steam injector when the steam valve is opened before the liquid valve, even if the drain is connected to the condenser with a high depressurization.

4. Experimental results and sensibility study

In this part, we study the influence of three important parameters: one geometrical parameter, the mixing section outlet diameter and two physical parameters, the inlet steam pressure and inlet liquid temperature. In all cases, the liquid inlet pressure ($P_{0\,l}$) is equal to 1.3 bar and the vapour quality is equal to 0.95.

Table 1
Parameter ranges

Port	Independent parameters	Dependent parameters
Steam	$P_{0\,s}$:1–12 bar	$x_{0\,s} = 0.95$–1.0; $\dot{m}_s = 0$–500 kg/h
Liquid	$T_{0\,l}$:15–110°C; $P_{0\,l}$: 0–20 bar	$\dot{m}_l = 15000$ kg/h
Discharge	$P_{3\,l}$: 0–20 bar	—

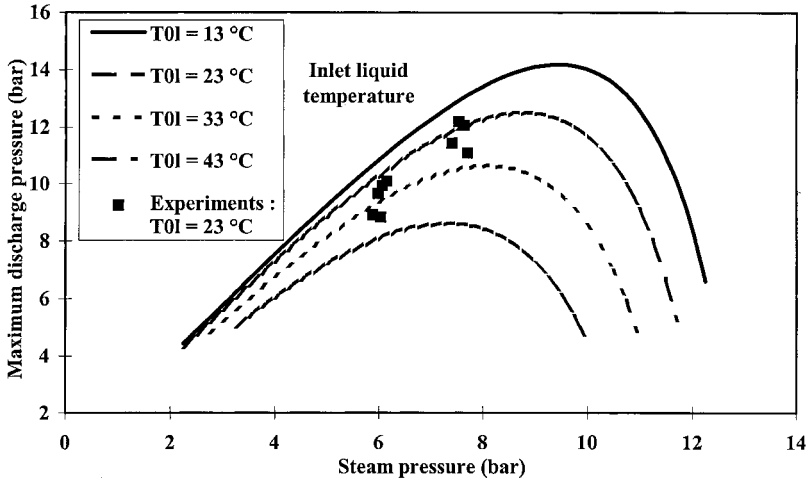

Fig. 10. Effect of inlet liquid temperature on discharge pressure ($P_{0\,1}$ = 1.3 bar; Ω = 1/12).

4.1. Influence of the liquid temperature on the injector performance

The injector performance is represented by the maximum discharge pressure at the exit of the injector as a function of the steam inlet pressure. Fig. 10 shows the efficiencies for different water inlet temperatures. The increase of the temperature leads to a fast degradation of performance and decreases the working range of the injector.

The maximum water temperature, for the desired functioning condition ($P_{0\,1}$ = 1.3 bar, vapour quality = 0.95) is equal to 55°C. Good agreement is obtained between experimental results and computed values. The accuracy of the model is about 15%.

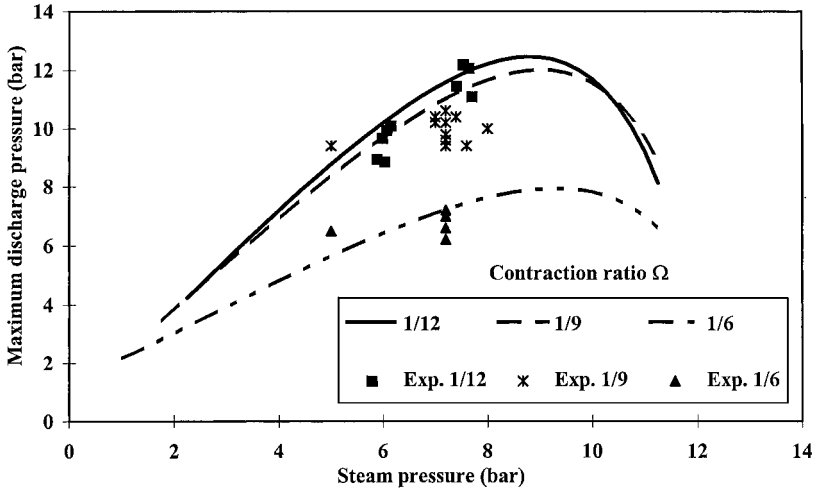

Fig. 11. Effect of contraction ratio on discharge pressure ($P_{0\,1}$ = 1.3 bar; $T_{0\,1}$ = 20°C).

4.2. Influence of throat diameter on the injector performance

One key aspect of the injector design is the mixing section ratio Ω (Fig. 11). This parameter determines the maximum discharge pressure and the working range of the injector. For high contraction ratios, high discharge pressures can be reached but the working range decreases. This conclusion has been experimentally verified.

The model is able to predict:

- the maximum ratio Ω for which the injector is able to operate for fixed liquid inlet conditions. For $P_{0\,1} = 1.3$ bar and $T_{0\,1} = 15°C$, the maximum ratio is 1/17.3;
- for fixed functioning limits or discharge pressure respectively, the maximum or the minimum mixing section ratio.

5. Conclusion

In this study, a simple global model is developed. This modelling only requires one empirical closure equation and is able to predict the influence of different geometrical parameters of the injector (mixing section throat diameter, position of the liquid pipe, etc.) and the influence of physical parameters (temperature, liquid and steam pressure, etc.) on the injector performance, with an accuracy of about 15%.

A test facility was designed and built at CETHIL. This experimental study permitted the validation of the model in several geometric configurations and for several inlet parameters.

The study shows that steam-injectors can be used in many applications, particularly for security water injection in steam generators of nuclear reactors.

References

Alad'yev, I.T., Krantov, F.M., Teplov, S.V., 1981a. Experimental study of flow in the mixing chamber of an injector. Fluid Mech. Sov. Res. 10, 92–103.

Alad'yev, I.T., Kabakov, V.I., Teplov, S.V., 1981b. Investigation of a multijet injector at different ratios of the velocities of the mixing stream and different areas of the mixing chamber exit. Fluid Mech. Sov. Res. 10, 116–125.

Cattadori, G., Galbiati, L., Mazzocchi, L., Vanini, P., 1991. A single-stage high pressure steam injector for next generation reactors. Test results and analysis. Int. J. Multiphase Flow 21, 591–606.

Grolmes, A., 1968. Steam–water condensing-injector performance analysis with supersonic inlet vapor and convergent condensing section. Argonne National Laboratory, Argonne (USA), report ANL-7443.

Idel'cik, I.E., 1986. Memento des pertes de charge. Eyrolles, Paris.

Leone, J.F., Chisacof, A., Lallemand, A., 1994. Pompe à injection de vapeur. Etude expérimentale. Congrès SFT, Paris, pp. 149–154.

Leone, J.F., Rodet, J.C., Lallemand, A., 1995. Entraînement d'un liquide par un jet de vapeur. In: Application aux pompes à injection de vapeur. JITH, Marrakech (Maroc), pp. 537–549.

Manno, V.P., Dehbi, A.A., 1990. A note: a model of steam injector performance. Chem. Engng Commun. 95, 107–119.

Myasaki, K., Nakajima, I., Fujii, E. et al, 1973. Condensing heat transfer in steam water steam injector. J. Nucl. Sci. Technol. 10, 411–418.

Narabayashi, T., Ishiyama, T., Miyano, H., Nei, H., Shioiri, A., 1991. Feasibility and application on steam injector for next-generation reactor. 1st JSME/ASME Joint International Conference on Nuclear Engineering. Tokyo, pp. 23–28.

Rose, R.P., 1960. Steam jet pump analysis and experiments. Westinghouse Electric corporation. Pittsburgh, report WAPD-TM-227.

Saltanov, G.A., Tsiklauri, G.V., Shanin, V.K., 1970. Shock waves in a flow of wet vapour with high liquid phase content. Teplofisika Vysokikh Temperatur 8, 571–578.

Schmidt, E., 1969. Properties of Water and Steam in SI-Units. Springer, Berlin.

Young, J.B., Guha, A., 1991. Normal shock-wave structure in two-phase vapour-droplet flows. J. Fluid Mech. 228, 243–274.